IEEE Access
Multidisciplinary ⋮ Rapid Review ⋮ Open Access Journal

Received October 11, 2020, accepted November 4, 2020, date of publication November 9, 2020, date of current version November 19, 2020.

Digital Object Identifier 10.1109/ACCESS.2020.3036880

High Precision Self-Mixing Interferometer Based on Reflective Phase Modulation Method

LIPING LU[1], LU HU[1], ZHEN LI[1], LIRONG QIU[1], WENCAI HUANG[1], AND XIULIN WANG[2]
[1]Department of Electronics Engineering, Xiamen University, Xiamen 361005, China
[2]Department of Physics, Jimei University, Xiamen 361021, China

Corresponding author: Wencai Huang (huangwc@xmu.edu.cn)

This work was supported in part by the National Natural Science Foundation of China (NSFC) under Grant 61675174, and in part by the Natural Science Foundation of Fujian Province under Grant 2020J01705.

ABSTRACT In this paper, a novel self-mixing interferometer based on reflective phase modulation (RPM) method has been developed to perform micro-displacement reconstruction with nanometer accuracy. Broaden harmonic components spectrum of the self-mixing signal is produced by employing a high-frequency vibrating reflective mirror as the phase modulation device. Phase demodulation is implemented applying the orthogonal demodulation algorithm subject to the signal spectrum, in which orthogonal signal can be extracted from the harmonic components of the expanded Bessel function. The principle and signal processing approach are introduced in detail, and the simulation results indicate that the reconstruction error can be reduced as the number of reflections increases. A series of experiments at different vibration amplitudes show that the reconstructed errors are all less than 10 nm with modulation frequency of 1 kHz. And the minimum error of 3 nm has been achieved at the measured amplitude of 229 nm, which demonstrates the technical-superiority and high-performance of the method.

INDEX TERMS Phase modulation, self-mixing interference, micro-displacement measurement.

I. INTRODUCTION

From 1967, Peek firstly exploited the self-mixing interferometer (SMI) to measure variations in the optical path length and the behavior of lasers [1]. Due to its characteristics of inherent simplicity, compactness and self-alignment, SMI has been extensively used in many fields, such as distance [2], [3], displacement [4]–[6], velocity [7], [8], parameters of laser [9], [10], tomography [11], and biomedical signals [12]. As one fringe corresponding to half a wavelength displacement, it is convenient to reconstruct the target's vibration by fringe-counting method [13]. Another approach for reconstruction of external vibration is based on the phase unwrapping method [14], [15], which is able to achieve high reconstruction precision without depending on the number of fringes. However, in the actual experiments, the SMI system may be affected by various environmental factors such as noise and speckle effect, which will cause signal intensity fluctuation. In this case, the displacement of the external target can't be reconstructed accurately by using the phase unwrapping method. In order to eliminate the effect of the signal intensity fluctuation on the phase unwrapping method, the phase modulation is introduced into SMI technology. In 2006, Guo and Wang [16] employed an electro-optic modulator (EOM) in an external cavity with a temporal-carrier phase-shifting technique that can effectively restore the vibration displacement of the target. However, when the modulation frequency is high, the triangular wave signal is prone to distortion, which causes measurement error and limits the measuring range. To solve this problem, Xia *et al.* [17] developed a sinusoidal phase-modulating SMI, which processed the interference signal in the frequency domain. The complete information of the interference signal was maintained and the sensitivity of the system to noises has been reduced. In 2017, Jiang *et al.* [18] combined the multiple self-mixing interference (MSMI) modulation with the four-quadrant integral technique, obtaining displacement reconstruction with higher accuracy. The sinusoidal phase modulation using EOM can greatly suppress the influence of low frequency and high frequency noises, thus provide a better signal-to-noise ratio (SNR). However, it requires high performance of polarized optical devices to eliminate the effect by the polarization state of light and increases the system's cost.

The associate editor coordinating the review of this manuscript and approving it for publication was Zhongyi Guo.

In this paper, we present a novel reflective phase modulation (RPM) method to reconstruct the displacement by placing a piezoelectric transducer (PZT) with high-frequency vibration in the external cavity. The high-frequency PZT plays as phase modulation device. This method effectively combines phase modulation with multiple reflection technique [19] for the micro-vibration measurement. The phase of the modulated signals is calculated by extracting the first and second harmonic signals in the frequency domain, and the displacement of the vibrating target can be reconstructed according to it. Due to the combination of multiple reflection technology, the proposed method is able to realize high-precision displacement reconstruction for weak vibration far less than half a wavelength. In addition, this method has the superiority of scalable precision by increasing the number of reflections that make it have potential applications in sub-nanometer precision measurement.

II. THEORETICAL ANALYSIS

Self-mixing interference (SMI) is a phenomenon that part of laser light reflected or back-scattered by the external target re-injects the resonant cavity and re-coupled to the laser's cavity, which results in fluctuations of power and the frequency of the laser. The academic theory of SMI has been thoroughly researched and discussed by [20]–[22]. According to the three- facet Fabry-Pe'rot model, the transmitted power P can be expressed as:

$$P = P_0 \left(1 + m \cos \phi_F\right) \tag{1}$$

The laser phase is subject to the feedback given by the phase equation:

$$\phi_F = \phi_0 - C \sin \left(\phi_F + \arctan \alpha\right) \tag{2}$$

in the Eq.(1) and (2), P_0 is the laser power without optical feedback, and m is the modulation index. Meanwhile, α is line width enhancement factor and C is optical feedback factor which indicates the level of the external optical feedback. ϕ_0 ($\phi_0 = 2kL = 4\pi L/\lambda$) and ϕ_F respectively represent the optical phase of the laser without and with light feedback, where k is the wave number, λ is the wavelength and L is the variation of distance from the LD to the target. In the weak feedback region ($0 < C < 1$), the phase equation has a single solution, which means laser is in a single-mode state. As a result, ϕ_F varies little, it can still be approximated as a phase signal without optical feedback. In other words, $\phi_F \approx \phi_0$.

In Ref. [19], by employing a simple external reflecting mirror, the light re-injected back into the laser after zigzag reflections between two reflecting mirrors. In this case, the optical path augments with the same displacement of the target, inducing the improvement of measurement precision. And the gain of optical path $G(N, \theta)$ can be derived through the geometric calculation of the optical path, it can be given as:

$$G(N, \theta) = \begin{cases} 1, & N = 1 \\ \dfrac{1}{\cos(\theta)} + \displaystyle\sum_{n=1}^{N-1} \dfrac{\cos \frac{N\theta}{N-1}}{\cos \frac{(n-1)\theta}{N-1} \cos \frac{n\theta}{N-1}}, & N \geq 2 \end{cases} \tag{3}$$

where N ($N \geq 2$) is the number of reflections and θ is the laser incident angle. Actually, the optical path gain $G(N, \theta)$ is the actual optical path generated by the vibration of the target divided by the original vibration displacement. After deeply analyzed, it has been concluded that the closer the value of θ is to 10°, the larger the maximum measurable displacement and the smaller the error [19]. Thus, the value of the incident angle is set to be 10° in our next simulations and experiments.

In this paper, a novel RPM method is designed based on the above external reflecting mirror model, the diagrammatic sketch of system is shown in Fig. 1. In the design, the target M_1 vibration is $S(t) = A \sin(2\pi f_0 + \beta)$, an external mirror M_2 is driven to vibrate as $H(t) = B \sin(2\pi f_w + \gamma)$ simultaneously, where A, B and f_0, f_w are the amplitudes and the frequencies of M_1, M_2 respectively. In the schematic, ray propagation analysis shows that compared with the path of the laser re-injecting into the resonant cavity when the external mirror M_2 is static, the actual advance in optical path is no longer related to the vibration of M_1 alone, then the actual optical path $L(N, \theta)$ can be figured out by geometric calculation:

$$L(2, \theta) = 2 \cos \theta * S + H \tag{4}$$

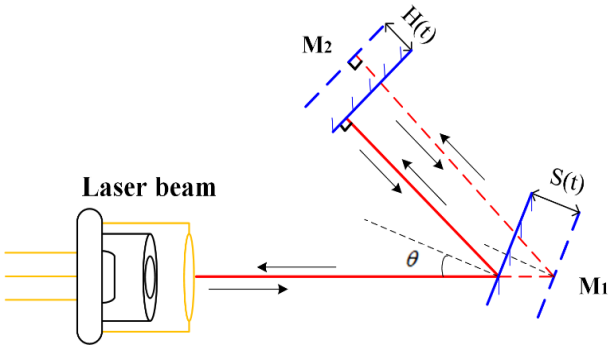

FIGURE 1. Schematic of reflective phase modulation method optical path.

Accordingly, as the number of reflections increases, the same analysis can be easily adapted to obtain the following formula:

$$L(3, \theta) = (2 \cos \theta + 1) * S + 2 \cos \frac{\theta}{2} * H \tag{5}$$

After reflected by M_1, the first incident angle of the light on M_2 is θ_2, which is defined as the angle between the incident light and the normal. For example, as shown in Fig.1, when the light is incident perpendicular to M_2, the incident light coincides with the normal, thus $\theta_2 = 0$. In principle, as long

as there is a laser perpendicular to M_1 or M_2 during the reflection process, the beam can be reflected between the two mirrors with any propagating number. Through a series of angle analysis with larger reflections number and inductive recursion, we get the expression:

$$\theta_2 = \frac{(N-2)*\theta}{N-1} \tag{6}$$

Finally, a general formula can be derived by combining Eq. (4)-(6):

$$L(N,\theta) = G(N,\theta)*S + G(N-1,\theta_2)*H \tag{7}$$

Under the circumstances, laser power can be written as:

$$P = P_0\{1 + m\cos[\phi_F + \psi(t)]\} \tag{8}$$

with:

$$\phi_F = \frac{4\pi}{\lambda}*G(N,\theta)*S \tag{9}$$

$$\psi(t) = \frac{4\pi}{\lambda}*G(N-1,\theta_2)*H \tag{10}$$

At this point, we treat $\psi(t)$ as the sinusoidal phase modulation term, the sinusoidal phase modulation depth is $h = \frac{4\pi}{\lambda}*G(N-1,\theta_2)*B$. Expanding Eq. (8) by the Bessel function after DC blocking and normalization processing [13], [23], we obtain:

$$\begin{aligned} P = {} & \cos(\phi_F) J_0(h) + 2\cos(\phi_F) \\ & \times \sum_{n=1}^{\infty} J_{2n}(h)\cos[(2n)(2\pi f_w t + \gamma)] - 2\sin(\phi_F) \\ & \times \sum_{n=1}^{\infty} J_{2n-1}(h)\cos[(2n-1)(2\pi f_w t + \gamma)] \end{aligned} \tag{11}$$

Here, $J_n(h)$ is the first type Bessel function of order n with the independent variable b, $J_{2n}(h)$ and $J_{2n-1}(h)$ are the even and odd orders, respectively. As can be seen that the AC component of the SMI signal is composed of the fundamental frequency f_w and its harmonics, and the odd harmonics fluctuate with $\sin(\phi_F)$ while the even harmonics fluctuate with $\cos(\phi_F)$. Furthermore, ϕ_F can be solved by comparing the amplitudes of two considerable low-order frequency components shown as the following expression [17]:

$$\phi_F = \arctan\left[\frac{J_2(h)*C_1(t)}{J_1(h)*C_2(t)}\right] \tag{12}$$

Here, $C_1(t)$ and $C_2(t)$ respectively represent the amplitudes of first and second harmonics. Obviously, after an unwrap process, we obtain continuous value of ϕ_F. Ultimately, the variation information of the external target M_1 can be deduced by combining Eq. (9) and Eq. (12):

$$S(t) = \arctan\left[\frac{J_2(h)*C_1(t)}{J_1(h)*C_2(t)}\right]*\frac{\lambda}{4\pi*G(N,\theta)} \tag{13}$$

The flow chart used to perform the displacement reconstruction is shown in Fig.2.

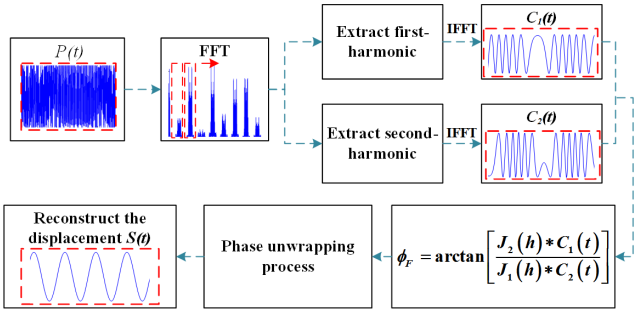

FIGURE 2. Flow chart of the method.

III. SIMULATION RESULTS

Based on the above description of the reflective phase modulation system, a series of simulations with different parameters have been carried out to verify the feasibility of the method. Primarily, the simple harmonic motion signal of M_1 and M_2 is simulated at $A = 0.4\ \mu m$, $f_0 = 10Hz$, $B = 1\ \mu m$, $f_w = 1000Hz$, $\lambda = 650nm$, $\theta = 10^o$, $\alpha = 6$, $C = 0.2$, and $N = 2$. The displacement reconstruction process is consistent with the flowchart Fig.2. Simulated result is shown in Fig.3. Fig.3(a) is the phase-modulated SMI signal when target M_1 and external reflecting mirror M_2 vibrating simultaneously. After Fourier transform processing, the frequency spectrum of signal is illustrated in Fig.3(b). It is obvious that the spectrum of the signal is distributed to fundamental frequency components and harmonic components locating in integer multiples of 1000, which is consistent with the results obtained by theoretical analysis. After extracting the first and second harmonics by two filters in the frequency domain, it is easy to obtain the wrapped phase by inverse Fourier transform and mathematical computation as in Eq. (11), the calculation result is shown in Fig.3(c). Ultimately, the variation information of the external target, as shown in Fig.3(d), can be measured from wrapped phase and the reconstructed result (in blue) is very close to the real displacement (in red) set by the simulation. Then, several simulations with different amplitudes are carried out and the results verified the feasibility of this method.

In order to further illustrate the relationship between accuracy of system and the number of reflections N, we perform simulations that increase the number of reflections N to 3 without changing other parameters. Fig.4 shows the comparison of simulation results for $N = 2$ and $N = 3$. Figs.4(a)-4(d) and Figs. 4(e)-4(h) show the signal frequency spectrum, extracted phase, the reconstructed displacement, and the displacement reconstruction error for these two cases, respectively. Fig.4(a) and Fig.4(e) clearly demonstrate that the increase in the number of reflections N results in a broadening spectrum of harmonic components. Consequently, a higher reconstruction accuracy will be obtained. As can be seen from Fig.4(d) and Fig.4(h), the reconstruction error with $N = 3$ is about 5nm which is almost half of that with $N = 2$. Further simulations of larger number of reflections N indicate that reconstruction accuracy is scalable with the increase of N.

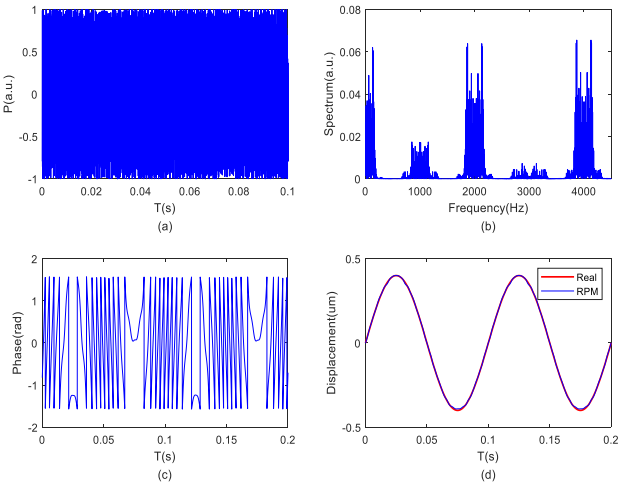

FIGURE 3. Realization of interference signal processing. (a) Simulated phase modulating SMI signal with $N = 2$. (b) Frequency spectrum of SMI signal. (c) Extracted phase from SMI. (d) Reconstructed displacement.

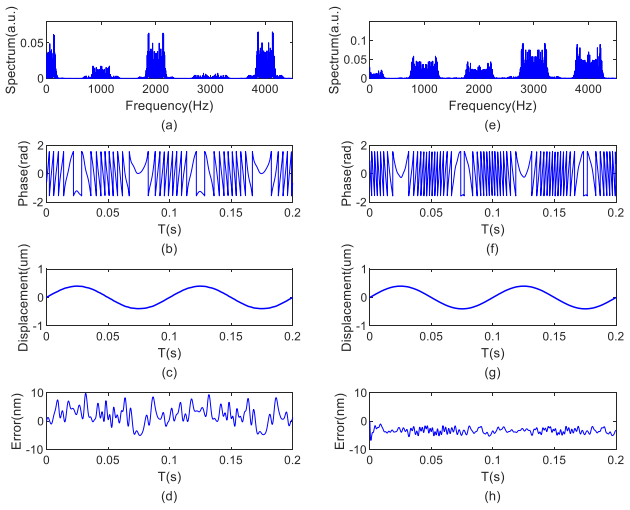

FIGURE 4. Displacement reconstruction results with $N = 2$ and $N = 3$. (a) Frequency spectrum of SMI signal ($N = 2$). (b) Extracted phase from SMI signal ($N = 2$). (c) Displacement reconstruction of SMI ($N = 2$). (d) Displacement reconstruction error of SMI ($N = 2$). (e) Frequency spectrum of SMI signal ($N = 3$). (f) Extracted phase from SMI ($N = 3$). (g) Displacement reconstruction of SMI ($N = 3$). (h) Displacement reconstruction error of SMI ($N = 3$).

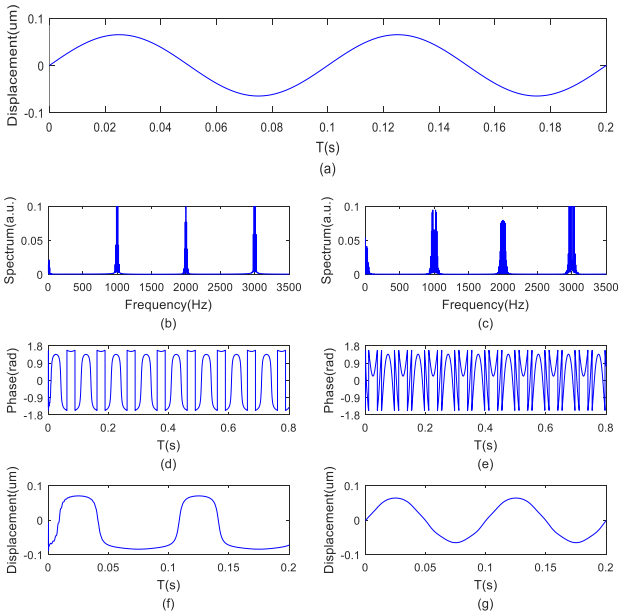

FIGURE 5. Simulation results of different methods with $A = \lambda/10$. (a) Simulated displacement of the external target. (b) Frequency spectrum of SMI signal with EOM phase modulation. (c) Frequency spectrum of SMI signal with RPM method. (d) Extracted phase from SMI of EOM phase modulation. (e) Extracted phase from SMI of RPM method. (f) Displacement reconstruction of EOM phase modulation. (g) Displacement reconstruction of RPM method.

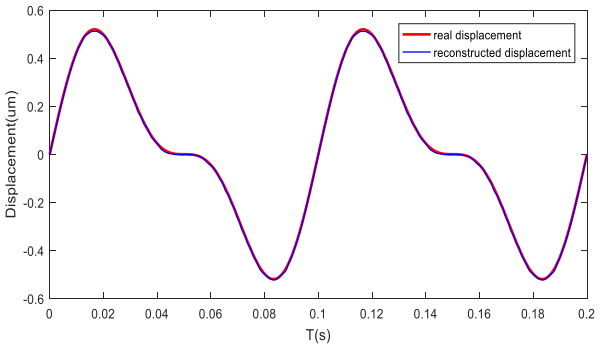

FIGURE 6. Simulation results for arbitrary wave motion.

To illustrate the superiority of the proposed RPM method, the simulation has been conducted when the external vibration amplitude is reduced to $\lambda/5(A = \lambda/10)$. Fig.5(a) is the simulated sinusoidal displacement of the external target. Fig.5(b) shows the generated SMI signal spectrum by EOM phase modulation method. It can be seen clearly that the weak vibration results in excessively narrow harmonic components. Consequently, it will lead to the error of the extracted phase and failure of reconstruction, as shown in Fig.5(d) and Fig.5(f). Apparently, employing the proposed RPM method with $N = 3$ results in a broadening spectrum of harmonic components, as shown in Fig.5(c). As a result, the weak vibration far less than half a wavelength can be successfully reconstructed by the RPM method, which corresponding to Fig.5(g). In addition, the simulation of random displacement reconstruction is performed in order to better show the RPM method could be powerful in such a case. As shown in Fig.6, the real displacement (in red) and the reconstructed displacement (in blue) for the method show a strong overlap. It illustrates that the proposed RPM method is not limited to the displacement reconstruction of sinusoidal vibration, and is applicable for other forms of wave motion as well.

IV. EXPERIMENTAL SETUP AND RESULTS

In order to confirm the validity of the proposed phase modulation method, a series of experiments have been performed. The experimental setup is shown in Fig.7. We use

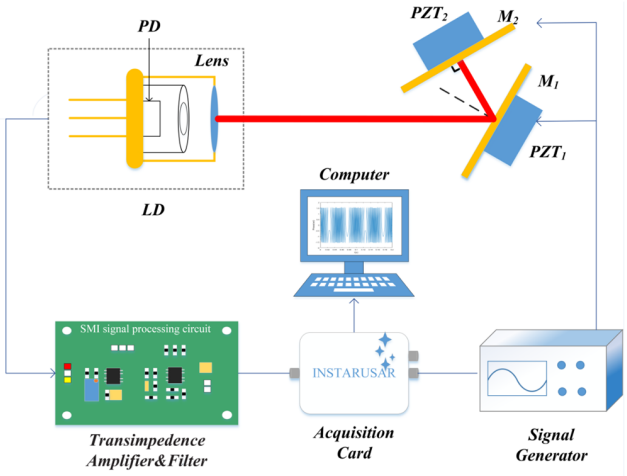

FIGURE 7. Setup of the experiment system.

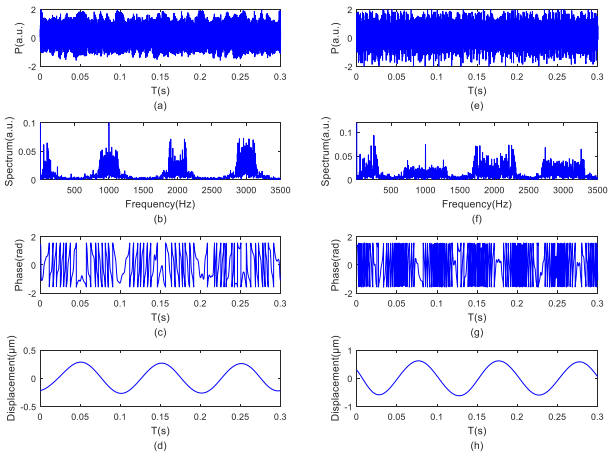

FIGURE 8. Experimental results with the driving voltage 7V and 15V of PZT_1. (a) Phase-modulated SMI signal (7V). (b) Frequency spectrum of SMI signal (7V). (c) Extracted phase from SMI (7V). (d) Reconstructed displacement (7V). (e) Phase-modulated SMI signal (15V). (f) Frequency spectrum of SMI signal (15V). (g) Extracted phase from SMI (15V). (h) Reconstructed displacement (15V).

a LD (FU650AD5_C9N) as the light source, emitting up to 5 mW at 650 nm on a single longitudinal mode, driven by a constant current supply. The external cavity is composed of two PZTs (driven by AFG3022 signal generator) pasted with mirrors M_1 and M_2 respectively. The PZT_2 with higher frequency plays the role of phase modulation, and the low-frequency PZT_1 represents the target to be measured. The angle between M1 and M_2 is adjusted carefully to achieve multiple reflections under the premise that the collimated beam re-enters the laser cavity. The changes of laser power are detected by a power-monitor Photodetector (PD) packaged in the LD and transformed into current, which will be amplified by a transimpedance amplifier and acquired by a computer via Data acquisition card (DAQ card) (ISDS205A). A commercial interferometer (LV-IS01, SOPTOP) with 0.15 nm resolution was used to test the displacement of the same target (PZT_1) for comparison.

As the same of simulations, Sinusoidal motions are performed with two PZTs. Two experiments with different driving voltages were carried out. The PZT_2 is driven with a driving voltage of 15 Vpp and frequency of 1 kHz, while the frequency of PZT_1 is set to 10 Hz with different driving voltages. Then, the external mirror M_2 is adjusted vertically to make the laser beam reflect two times and ensure the laser beam reflected back to the laser cavity. Fig.8 shows experimental results with the different driving voltage (7V and 15V) of PZT_1. Figs.8(a)-8(d) and Figs. 8(e)-8(h) show the phase-modulated SMI signal, the signal frequency spectrum, extracted phase and the reconstructed displacement for these two cases, respectively. It can be seen from Figs.8(b) and Figs.8(f) that, since the frequency of the modulation mirror remains unchanged, the center of the first and second harmonic components are 1kHz and 2kHz respectively. In addition, the frequency spectrum is obviously broaden caused by amplitude increasing.

In order to illustrate the superiority of the proposed RPM method, the comparable experiments by using the EOM phase modulation are carried out. The vibration frequency of the target (PZT_1) is set to 10Hz, and the driving voltage is 15 Vpp. The modulation frequency of EOM is 1kHz, and it's driving voltage is set to half-wave voltage of 6.75 Vpp. Fig.9(a) shows the obtained SMI signal

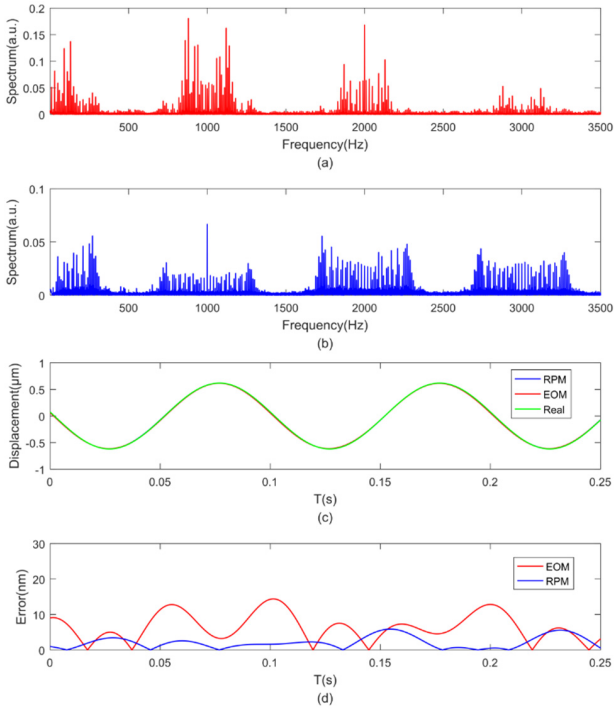

FIGURE 9. Experimental displacement reconstruction results with different methods. (a) Frequency Spectrum of EOM phase modulation. (b) Frequency spectrum of RPM. (c) Reconstructed displacement. (d) Reconstruction error.

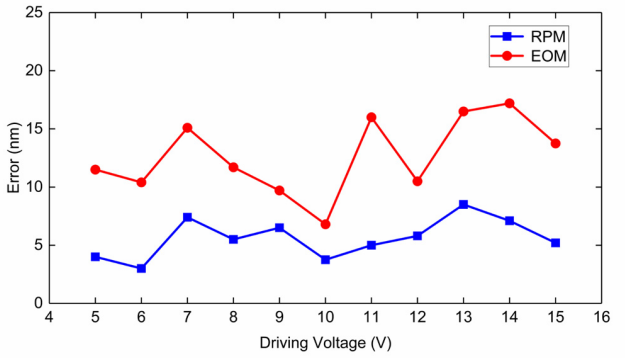

FIGURE 10. Experimental errors of the proposed RPM (in blue) and EOM phase modulation methods (in red) with different driving voltages.

spectrum generated by EOM phase modulation method. The corresponding reconstructed displacement is shown as the red curve in Fig.9(c). Then, the PZT_2 with driving voltage of 15Vpp and frequency of 1kHz is used for the reflective phase modulation. Fig.9(b) shows the SMI signal spectrum by using the proposed RPM method. It can be observed that the spectrum of harmonic components is significantly broadened due to multiple reflections. The reconstructed displacement with RPM method is shown as the blue curve in Fig.9(c). The green curve in Fig.9(c) represents the real displacement. As can be seen from Fig.9(d), the maximum reconstruction error of RPM method (in blue) is 5.9nm, while that of EOM phase modulation method (in red) is 15.7nm. The experimental results indicate that employing RPM method has higher accuracy as compared with that by the EOM phase method.

In addition, several experiments with different vibration amplitudes were performed. The driving voltage of PZT_1 is changing from 5 to 15 Vpp with a step interval of 1 Vpp, and other parameters are kept the same as those in the preceding experiment. In order to ensure the reliability of the experiment, the reconstruction displacement under each driving voltage is measured repeatedly. The average value of errors by the proposed RPM and EOM phase modulation methods are shown in Fig.10, respectively. It can be observed that the errors of RPM method are all within 10nm. The comparison indicates that the reconstruction accuracy of RPM is higher than that of EOM phase modulation method.

V. CONCLUSION

In conclusion, we have demonstrated a novel reflective phase modulation (RPM) method to realize high precision displacement reconstruction. The phase modulation is conducted by using a high-frequency vibrating reflective mirror that can perform multiple reflections simultaneously. Simulations and experiments both illustrate the superiority of the method. Moreover, the spectrum of harmonic components can be further broadened by increasing the number of reflections, so that the displacement of weak vibration far less than half a wavelength can be accurately reconstructed. Therefore, the proposed method has the advantages of scalable precision, broad measuring range and low cost, which makes it particularly important in the fields of high precision and nanoscale vibration monitoring.

ACKNOWLEDGMENT

(Liping Lu and Lu Hu contributed equally to this work.)

REFERENCES

[1] T. H. Peek, P. T. Bolwijn, and C. T. J. Alkemade, "Axial mode number of gas lasers from moving-mirror experiments," *Amer. J. Phys.*, vol. 35, no. 9, pp. 820–831, Jan. 1967.
[2] D. Guo and M. Wang, "Self-mixing interferometry based on a double-modulation technique for absolute distance measurement," *Appl. Opt.*, vol. 46, no. 9, pp. 1486–1491, Mar. 2007.
[3] A. Magnani, A. Pesatori, and M. Norgia, "Real-time self-mixing interferometer for long distances," *IEEE Trans. Instrum. Meas.*, vol. 63, no. 7, pp. 1804–1809, Jul. 2014.
[4] Y. Fan, Y. Yu, J. Xi, and J. F. Chicharo, "Improving the measurement performance for a self-mixing interferometry-based displacement sensing system," *Appl. Opt.*, vol. 50, no. 26, pp. 5064–5072, Sep. 2011.
[5] K. Zhu, B. Guo, Y. Lu, S. Zhang, and Y. Tan, "Single-spot twodimensional displacement measurement based on self-mixing interferometry," *Optica.*, vol. 4, no. 7, pp. 729–735, Jul. 2017.
[6] C. Bes, G. Plantier, and T. Bosch, "Displacement measurements using a self-mixing laser diode under moderate feedback," *IEEE Trans. Instrum. Meas.*, vol. 55, no. 4, pp. 1101–1105, Aug. 2006.
[7] O. D. Bernal, U. Zabit, F. Jayat, and T. Bosch, "Sub-λ/2 displacement sensor with nanometric precision based on optical feedback interferometry used as a non-uniform event-based sampling system," *IEEE Sensors J.*, vol. 20, no. 10, pp. 5195–5203, May 2020.
[8] B. Gao, C. Qing, S. Yin, C. Peng, and C. Jiang, "Measurement of rotation speed based on double-beam self-mixing speckle interference," *Opt. Lett.*, vol. 43, no. 7, pp. 1531–1533, Apr. 2018.
[9] G. Giuliani, M. Norgia, S. Donati, and T. Bosch, "Laser diode self-mixing technique for sensing applications," *J. Opt. A, Pure Appl. Opt.*, vol. 4, no. 6, pp. S283–S294, Nov. 2002.
[10] Y. Zhao, J. Zhou, and L. Lu, "Measurement of the free spectral range of the laser cavity based on multi-longitudinal mode laser self-mixing vibrator," *Measurement*, vol. 135, pp. 467–472, Mar. 2019.
[11] Y. Tan, W. Wang, C. Xu, and S. Zhang, "Laser confocal feedback tomography and nano-step height measurement," *Sci. Rep.*, vol. 3, no. 1, Oct. 2013, Art. no. 2971.
[12] S. Donati and M. Norgia, "Self-mixing interferometry for biomedical signals sensing," *IEEE J. Sel. Topics Quantum Electron.*, vol. 20, no. 2, pp. 104–111, Mar./Apr. 2014.
[13] S. Donati, G. Giuliani, and S. Merlo, "Laser diode feedback interferometer for measurement of displacements without ambiguity," *IEEE J. Quantum Electron.*, vol. 31, no. 1, pp. 113–119, Jan. 1995.
[14] Z. Huang, C. Li, and X. Sun, "Piece-wise transition detection algorithm for a self-mixing displacement sensor," *Chin. Opt. Lett.*, vol. 11, no. 9, pp. 091203-8–091203-12, Sep. 2013.
[15] A. Ehtesham, U. Zabit, O. D. Bernal, G. Raja, and T. Bosch, "Analysis and implementation of a direct phase unwrapping method for displacement measurement using self-mixing interferometry," *IEEE Sensors J.*, vol. 17, no. 22, pp. 7425–7432, Nov. 2017.
[16] D. Guo and M. Wang, "Self-mixing interferometer based on temporal-carrier phase-shifting technique for micro-displacement reconstruction," *Opt. Commun.*, vol. 263, no. 1, pp. 91–97, Jul. 2006.
[17] W. Xia, M. Wang, Z. Yang, W. Guo, H. Hao, and D. Guo, "High-accuracy sinusoidal phase-modulating self-mixing interferometer using an electro-optic modulator: Development and evaluation," *Appl. Opt.*, vol. 52, no. 4, pp. B52–B59, Feb. 2013.
[18] C. Jiang, X. Wen, S. Yin, and Y. Liu, "Multiple self-mixing interference based on phase modulation and demodulation for vibration measurement," *Appl. Opt.*, vol. 56, no. 4, pp. 1006–1011, Feb. 2017.
[19] L. Wang, X. Luo, X. Wang, and W. Huang, "Obtaining high fringe precision in self-mixing interference using a simple external reflecting mirror," *IEEE Photon. J.*, vol. 5, no. 3, Jun. 2013, Art. no. 6500207.
[20] W. M. Wang, W. J. O. Boyle, K. T. V. Grattan, and A. W. Palmer, "Self-mixing interference in a diode laser: Experimental observations and theoretical analysis," *Appl. Opt.*, vol. 32, no. 9, pp. 1551–1558, Mar. 1993.

[21] R. Lang and K. Kobayashi, "External optical feedback effects on semiconductor injection laser properties," *IEEE J. Quantum Electron.*, vol. QE-16, no. 3, pp. 347–355, Mar. 1980.
[22] W. M. Wang, K. T. V. Grattan, A. W. Palmer, and W. J. O. Boyle, "Self-mixing interference inside a single-mode diode laser for optical sensing applications," *J. Lightw. Technol.*, vol. 12, no. 9, pp. 1577–1587, Sep. 1994.
[23] X. Dai, M. Wang, Y. Zhao, and J. Zhou, "Self-mixing interference in fiber ring laser and its application for vibration measurement," *Opt. Express*, vol. 17, no. 19, pp. 16543–16548, Sep. 2009.

LIPING LU received the bachelor's degree in electronic information engineering from Xiamen University, in 2018, where she is currently pursuing the master's degree. Her research interests include laser sensing and photoelectric signal processing.

LU HU received the bachelor's degree in electronic information engineering from the Wuhan University of Technology, in 2018. She is currently pursuing the master's degree with Xiamen University. Her research interests include signal processing and photoelectric sensing.

ZHEN LI received the bachelor's degree in optical information science and technology from Jimei University, in 2018. He is currently pursuing the master's degree with Xiamen University. His research interests include laser sensor and data processing.

LIRONG QIU received the bachelor's degree in electronic information engineering from Nanchang University, in 2019. He is currently pursuing the M.E. degree with the School of Electronic Science and Technology, Xiamen University. His research interests include optical sensing and data processing.

WENCAI HUANG received the Ph.D. degree in optics from the University of Science and Technology of China, Hefei, China, in 2003. From 2008 to 2009, he was a Visiting Researcher with the Centre for Photonics and Photonic Materials, where he is involved with photonic crystal fiber under the supervision of Prof. Jonathan Knight. He is currently a Professor with the Department of Electronics Engineering, Xiamen University, Xiamen, China. He is the author of over 50 publications in refereed journals and conference proceedings. His research interests include laser self-mixing interferometer and its applications, fiber optics communication devices, and ultrashort pulse lasers based on PCF.

XIULIN WANG received the Ph.D. degree in optics from Xiamen University, Xiamen, China, in 2009. She is currently a Professor with the Department of Physics, Jimei University, Xiamen. She has published nearly 30 technical papers in international journals and conferences. Her research interests include optical sensors, superfluorescent fiber source, and other fiber-based optical devices.